# OPTICAL CHARACTERIZATION OF AMORPHOUS SILICON HYDRIDE FILMS\*

G. D. CODY, C. R. WRONSKI, B. ABELES, R. B. STEPHENS and B. BROOKS Exxon Research and Engineering Company, Corporate Research Laboratories, Linden, N.J. 07036 (U.S.A.)

## Summary

The performance of solar cells can be approached from the view of optical limitations (the adsorbed solar photon) or electrical limitations (the collected carriers). In this paper we focus on the optical behavior of a-SiH<sub>x</sub> films and through these data define the intrinsic optical limitations on the performance of a-SiH<sub>x</sub>. We present proven techniques for the extraction of the optical constants for thin films of a-SiH<sub>x</sub> on quartz over the absorption range  $10^{-1}$  -  $10^{6}$  cm<sup>-1</sup>. For the range  $10^{4}$  -  $10^{6}$  cm<sup>-1</sup> we define an optical gap  $E_{\rm G}$  from a plot of  $(\alpha E)^{1/2}$  against E for films of comparable thickness. We show the utility of this parameter for guiding materials research and we discuss its theoretical significance. Below  $E_{\rm G}$  we utilized both optical and photoconductivity data to establish a sharp exponential edge. For a-SiH<sub>x</sub> the edge has an activation energy that can be sample dependent and for our films it ranges from 0.05 to 0.10. The device implications of this exponential edge are discussed.

## 1. Introduction

The optical properties of a material are defined by the spectral dependence of its complex index of refraction:  $\tilde{n}(E) = n(E) + i\kappa(E)$ . From  $\tilde{n}(E)$  we can obtain  $\tilde{\epsilon}(E)$  through the relation  $\tilde{n}^2 = \tilde{\epsilon}$ . The imaginary part of  $\tilde{\epsilon} = \epsilon_1 + i\epsilon_2$  describes the fundamental optical excitations of the material.

For a complete description of the elementary excitations, information on  $\tilde{\epsilon}(E)$  is required over a wide range of photon energy E. This is usually accomplished for bulk samples through the Kramers-Kronig analysis of reflectivity data since transmission measurements are restricted to relatively narrow ranges in E because of the high optical absorption. For thin film

<sup>\*</sup>Paper presented at the Photovoltaic Material and Device Measurements Workshop, "Focus on Amorphous Silicon", San Diego, California, U.S.A., January 3 - 4, 1980.

samples, optical transmission can cover a broad energy range but, in highly absorbing material, reflectivity measurements cover a wider spectral range.

For a semiconductor the spectral region of major interest is that in the vicinity of the absorption edge since it supplies information on the optical gap  $E_G$  as well as on the density of states within the gap. For semiconductors that can be prepared in thin film form, transmission, absorption and reflection measurements can be appropriate tools to obtain  $\tilde{\epsilon}(E)$  over the energy region within several volts of the absorption edge.

A fundamental assumption of thin film measurements is that films prepared under identical preparation conditions exhibit an  $\tilde{\epsilon}(E)$  that is independent of the film thickness D. Thus surface absorption or scattering must be small with respect to volume contributions. This assumption is hard to verify but is no more serious than that associated with reflectivity measurements where the surface of a material is assumed to be identical with the bulk.

In addition to characterizing the semiconductor near its absorption edge,  $\tilde{n}(E)$  determines the optical absorption of any electro-optic device and defines the optical limitations on device performance.

In this paper we first present a variety of optical techniques that we found useful in measuring  $\tilde{n}(E)$  (hence  $\tilde{\epsilon}(E)$ ) in the vicinity of the absorption edge of thin semiconducting films. We focus on films of amorphous silicon hydride (a-SiH<sub>x</sub>) with thicknesses from 300 Å to 5  $\mu$ m.

Our films were obtained for the most part by the r.f. glow discharge decomposition of  $\mathrm{SiH_4}$  onto anodic substrates held at elevated temperatures [1]. We also report some data on films of a- $\mathrm{SiH_x}$  prepared by reactive sputtering [2]. Many of the data were obtained for films with the composition  $\mathrm{SiH_{0.16}}$  where the substrate temperature is 240 °C. Hydrogen concentrations were determined by the  $^{15}\mathrm{N^{-1}H}$  interaction [3]. Film fabrication and physical characterization will be described elsewhere [1]. Some of the optical data, and their theoretical interpretation, have been published in a previous paper [4].

Finally we use the optical constants for a-SiH $_x$  to simulate the optical absorption of realistic Schottky diodes through an exact thin film optical program. We thus define the fundamental optical limitations of the simple solar devices with respect to the direct air mass one (AM1) solar spectrum.

## 2. Thin film optics

The determination of  $\tilde{n}(E)$  for a thin film material requires two of the three possible measurements: transmission, reflection and absorption. It is facilitated by a fourth measurement: the direct measurement of the film thickness D. There are many routes to the extraction of  $\tilde{n}(E)$  from such measurements. We present an approach that has worked well for a-SiH<sub>x</sub> films on quartz substrates in the thickness range from 300 Å to 5  $\mu$ m in the photon energy range 1.3 - 4.0 eV.

The optics are defined by the schematic diagram shown in Fig. 1(a). Normal incidence is assumed throughout this paper. In Fig. 1(a) a film of

Fig. 1. (a) Optical configuration corresponding to eqn. (1) - eqn. (4); (b) optical configuration corresponding to eqn. (18) and eqn. (19).

thickness D and refractive index  $\widetilde{n}$  ( $\widetilde{n}_2 = \widetilde{n}$ ) is confined between two infinite half-spaces of real index  $n_1$  ( $n_1 = 1$ ) and  $n_3$  (for quartz  $n_3 \doteq 1.5$ ). The incident wave is directed toward the film from medium 1 and we define a reflection coefficient  $R_{\rm F}$ , a transmission coefficient  $T_{\rm F}$  and an absorption coefficient  $A_{\rm F}$ . By conservation of energy

$$A_{\mathrm{F}} + R_{\mathrm{F}} + T_{\mathrm{F}} = 1$$

It is a simple matter to show that

$$T_{\rm F} = \frac{n_1}{n_3} \mid \tilde{t} \mid^2 \tag{1}$$

$$R_{\rm F} = |\widetilde{r}|^2 \tag{2}$$

where

$$\tilde{t} = \tilde{t}_{12} \exp(i\tilde{Q}) \, \tilde{t}_{23} \tilde{Z} \tag{3}$$

$$\widetilde{r} = \widetilde{r}_{12} + \widetilde{t}_{12} \exp(\mathrm{i}\widetilde{Q}) \widetilde{r}_{23} \exp(\mathrm{i}\widetilde{Q}) \widetilde{t}_{21} \widetilde{Z}$$
(4)

Equations (1) and (2) are derived from time averaging the Poynting vector. Equations (3) and (4) can be obtained almost by inspection by considering the passage of a ray through the film. The quantity  $\tilde{Q}$  given by

$$\tilde{Q} = \frac{2\pi \tilde{n}_2 D}{\lambda} \tag{5}$$

accounts for the complex phase shift on one transit of the film. The quantity  $\tilde{Z}$  given by

$$\tilde{Z} = \{1 - \tilde{r}_{21} \exp(i\tilde{Q}) \, \tilde{r}_{23} \exp(i\tilde{Q})\}^{-1}$$
 (6)

takes into account multiple reflections within the film. The coefficients  $\tilde{r}_{ij}$  and  $\tilde{t}_{ij}$  are the reflection and transmission coefficients for the magnetic vector and are defined by

$$\widetilde{r}_{ij} = 1 - \widetilde{t}_{ij} = \frac{\widetilde{n}_i - \widetilde{n}_j}{\widetilde{n}_i + \widetilde{n}_j} \tag{7}$$

We next calculate eqn. (1) and eqn. (2) under various limiting conditions.

2.1. Low absorption regime (E  $\leq$  E<sub>G</sub>) with a coherent source

Here  $n \gg \kappa$  and  $n > n_3$ ,  $n_1$ . If  $\Delta \lambda$  is the spectral width of the source at wavelength  $\lambda$ , then  $\Delta \lambda \pi n D/\lambda^2 \ll 1$ . We define  $R_0^{-1/2} \equiv r_{21}$  and  $R_1^{-1/2} \equiv r_{23}$  where the reflection and transmission coefficients are real. We define  $\alpha \equiv 4\pi \kappa/\lambda$ . When the phase condition

$$\exp(2i\tilde{Q}) = (\pm) \exp(-\alpha D) \tag{8}$$

is met, we obtain under the above conditions  $T_{\rm F}(^{\rm MAX}_{\rm MIN})$  and  $R_{\rm F}(^{\rm MIN}_{\rm MAX})$  where

$$T_{\rm F}(_{\rm MIN}^{\rm MAX}) = \frac{(1 - R_0)(1 - R_1) \exp{(-\alpha D)}}{\{1 \mp (R_0 R_1)^{1/2} \exp{(-\alpha D)}\}^2}$$
(9)

and

$$R_{\rm F}(_{\rm MAX}^{\rm MIN}) = \frac{\left\{R_0^{-1/2} \mp R_1^{-1/2} \exp(-\alpha D)\right\}^2}{\left\{1 \mp (R_0 R_1)^{1/2} \exp(-\alpha D)\right\}^2}$$
(10)

When  $\alpha D = 0$ 

$$T_{\rm F}(_{
m MIN}^{
m MAX}) + R_{\rm F}(_{
m MAX}^{
m MIN}) = 1$$

and  $T_{\rm F}(^{\rm MAX}_{\rm MIN})$  occurs when  $4\pi nD/\lambda$  is an  $(^{\rm even}_{\rm odd})$  multiple of  $\pi$ . The film absorption is given by

$$A_{\rm F}(_{\rm MIN}^{\rm MAX}) = 1 - T_{\rm F}(_{\rm MIN}^{\rm MAX}) - R_{\rm F}(_{\rm MAX}^{\rm MIN})$$
 (11)

For  $\alpha D \ll 1$ 

$$A_{\rm F}(_{\rm MIN}^{\rm MAX}) = \alpha D \frac{(1 - R_0)(1 + R_1)}{\{1 \mp (R_0 R_1)^{1/2}\}^2}$$
 (12)

Finally the geometric mean or logarithmic average of  $R_{\rm F}({}_{\rm MAX}^{\rm MfN})$  is

$$\{R_{\rm F}({\rm MIN})R_{\rm F}({\rm MAX})\}^{1/2} = \frac{R_0 - R_1 \exp(-2\alpha D)}{1 - R_0 R_1 \exp(-2\alpha D)}$$
(13)

a form which is more linear in  $\exp(-2\alpha D)$  than eqn. (10) is for low values of  $R_0R_1$ .

2.2. Low absorption regime with an incoherent source ( $\Delta \lambda \pi nD/\lambda^2 \gtrsim 1$ )
As for the case discussed in Section 2.1,  $n \gg \kappa$ ,  $n > n_3$ ,  $n_1$  and the fringes are cancelled to give the incoherent result

$$T_{\rm F}({\rm I}) = \frac{(1 - R_1)(1 - R_0) \exp(-\alpha D)}{1 - R_0 R_1 \exp(-2\alpha D)} \tag{14}$$

$$R_{\rm F}(I) = R_0 + \frac{(1 - R_0)^2 R_1 \exp(-2\alpha D)}{1 - R_0 R_1 \exp(-2\alpha D)}$$
 (15)

and, for  $\alpha D \ll 1$ ,

$$A_{\rm F}(I) = \alpha D \frac{(1 - R_0)(1 + R_1)}{1 - R_0 R_1} \tag{16}$$

It is interesting to note that  $T_{\rm F}({\rm I}) = \{T_{\rm F}({\rm MAX})T_{\rm F}({\rm MIN})\}^{1/2}$  and  $A_{\rm F}({\rm I}) = \{A_{\rm F}({\rm MAX})A_{\rm F}({\rm MIN})\}^{1/2}$ . If transmission and absorption are plotted on logarithmic scales, adjacent fringes can be averaged to produce the incoherent forms eqns. (14) and (16) which are relatively insensitive to  $R_0$  and  $R_1$  in the denominator compared with eqns. (10) and (12). This technique of "averaging" adjacent fringes has computational as well as noise reduction advantages.

# 2.3. High absorption regime

Here  $n \approx \kappa$  and  $\alpha D \gtrsim 1$ . Under these circumstances eqn. (1) simplifies to

$$T_{\rm F} = |\widetilde{t}_{12}|^2 |\widetilde{t}_{23}|^2 \frac{\exp(-\alpha D)}{n_3} \tag{17}$$

and eqn. (2) to

$$R_{\rm F} = |\widetilde{r}_{12}|^2 \tag{18}$$

## 2.4. Substrate optics

Before we proceed to the utilization of these formulae we have to include the substrate in the transmission and reflection. The large thickness of the substrate implies the incoherent limit and we simply modify eqns. (13) and (14) to correspond to the situation shown in Fig. 1(b). We identify  $1-R_0$  with the transmitted power  $T_{\rm F}$ . We introduce the very small reflection coefficient  $R_3$  at the substrate-air interface. Thus we write

$$T_{\rm M} = CT_{\rm F} = \frac{1 - R_3}{1 - R_1 R_3} T_{\rm F} \tag{19}$$

$$R_{\rm M} = R_{\rm F} + \frac{T_{\rm F}^2 R_3}{1 - R_1' R_3} \tag{20}$$

where  $R_1$  is the reflectivity of the substrate-film interface  $(R_1' = |\tilde{r}_{32}|^2)$ . For low index substrates such as quartz or glass the quantity C = 0.97, and in the low transmission region where we utilize the reflectivity  $R_M = R_F$ .

# 2.5. Summary of thin film optics

We now summarize the equations that we have found most useful.

$$A_{\rm F} + R_{\rm F} + T_{\rm F} + 1 \tag{21}$$

 $T_{\rm M}(_{
m MIN}^{
m MAX}) = CT_{
m F}(_{
m MIN}^{
m MAX})$ 

$$= \frac{C(1-R_0)(1-R_1)\exp(-\alpha D)}{\{1\mp (R_0R_1)^{1/2}\exp(-\alpha D)\}^2}$$
(9a)

when  $n \gg \kappa$ ,  $n > n_3$ ,  $n_1$  and the light source is coherent  $(\Delta \lambda \pi n D/\lambda^2 \ll 1)$ . In eqn. (9a)

$$C = 0.97$$
  $n_3 \approx 1.5, n \approx 4$ 
 $R_0^{1/2} = r_{21}$ 
 $R_1^{1/2} = r_{23}$ 
 $\alpha = 4\pi\kappa/\lambda$ 
 $r_{ij} = \frac{n_i - n_j}{n_i + n_i}$ 

The maxima satisfy  $4\pi n(\lambda)D/\lambda = 2L\pi$  where  $L = 0, 1, 2, \ldots$  The minima satisfy the same condition where  $L = 1/2, 3/2, 5/2, \ldots$ 

$$A_{\rm F}(_{\rm MIN}^{\rm MAX}) + R_{\rm F}(_{\rm MAX}^{\rm MIN}) + T_{\rm F}(_{\rm MIN}^{\rm MAX}) = 1 \tag{11}$$

$$A_{\rm F}(_{\rm MIN}^{\rm MAX}) = \alpha D \frac{(1 - R_0)(1 + R_1)}{\{1 \mp (R_0 R_1)^{1/2}\}^2}$$
 (12)

when  $\alpha D \ll 1$ .

$$\{T_{\mathsf{M}}(\mathsf{MAX})T_{\mathsf{M}}(\mathsf{MIN})\}^{1/2} = CT_{\mathsf{F}}(\mathsf{I}) \tag{14a}$$

$$T_{\rm F}({\rm I}) = \frac{(1 - R_1)(1 - R_0) \exp(-\alpha D)}{1 - R_0 R_1 \exp(-2\alpha D)}$$
(14)

$$\{A_{\rm F}({\rm MAX})A_{\rm F}({\rm MIN})\}^{1/2} = A_{\rm F}({\rm I})$$

$$= \alpha D \frac{(1 - R_0)(1 + R_1)}{1 - R_0 R_1} \tag{16}$$

when  $\alpha D \ll 1$ .

$$T_{\rm M} = C |\tilde{t}_{12}|^2 |\tilde{t}_{23}|^2 \frac{\exp(-\alpha D)}{n_2} \tag{19}$$

$$R_{\rm M} = |\tilde{r}_{12}|^2 \tag{20}$$

when  $\alpha D \gg 1$  and where

$$\widetilde{r}_{ij} = \frac{\widetilde{n}_i - \widetilde{n}_j}{\widetilde{n}_i + \widetilde{n}_j}$$

$$\tilde{t}_{ij} = 1 - \tilde{r}_{ij}$$

These equations can be used with independent measurements of D to determine n and  $\kappa$  (and hence  $\widetilde{\epsilon}$ ) over a range of several volts around the absorption edge.

## 3. Experimental thin film optics

#### 3.1. Transmission measurements

We utilized a Carey 17 spectrometer in the range 2.5 - 0.3  $\mu$ m for films of a-SiH<sub>x</sub> 0.03 - 5  $\mu$ m thick. In the low absorption domain nD was derived

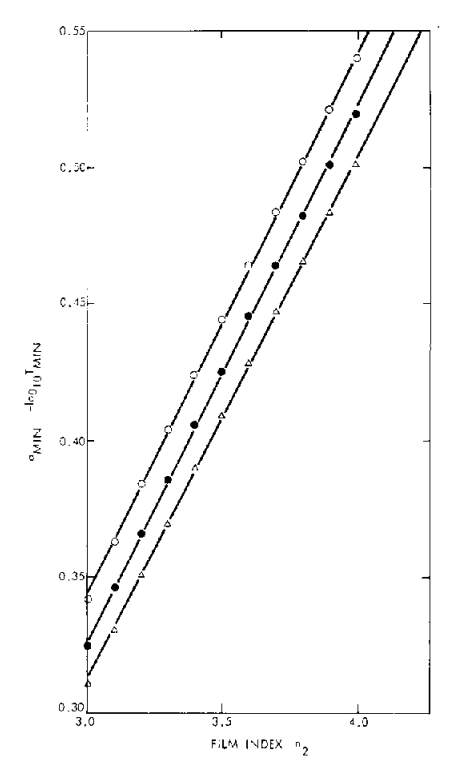


Fig. 2. The negative common logarithm of the transmission minimum in the fringe regime as a function of the film refractive index  $n_2$  and the substrate refractive index  $n_s$  corresponding to eqn. (9):  $\bigcirc$ ,  $n_s = 1.4$ ;  $\bullet$ ,  $n_s = 1.5$ ;  $\triangle$ ,  $n_s = 1.6$ .

from adjacent fringe pairs and was corrected to integer or half-integer multiples of  $2\pi$ . This measurement, combined with D, gave a value of n at  $\lambda \approx 2.5~\mu\text{m}$ . We also utilized  $T_{\rm M}({\rm MIN})$  (eqn. (9)) to infer the value, since as shown in Fig. 2 it is sensitive to the film index but not particularly sensitive to the substrate index. Conversely  $T_{\rm M}({\rm MAX})$  can be used to infer the substrate index (eqn. (9)).

The transmission of the film is only weakly dependent on the quantity n in the highly absorbing region (eqn. (19)) and we iterated reflectivity measurements (eqn. (18)) in this regime to obtain data on n and  $\kappa$ .

Finally, as discussed in Section 4, we were very successful in extending the transmission data to the region where  $\alpha D \approx 0.05$  - 0.5 by utilizing the logarithmic average of adjacent fringes in transmission through eqn. (14).

#### 3.2. Reflectivity measurements

Reflectivity measurements at normal incidence are difficult to accomplish on a Carey spectrometer. Our reflectivity attachment had an angle of incidence close to 20° and we did not control the polarization. We were able to compensate for these errors by referring the reflectivity of the amorphous silicon (a-Si) specimen to that of a standard calibrated at the Bureau of

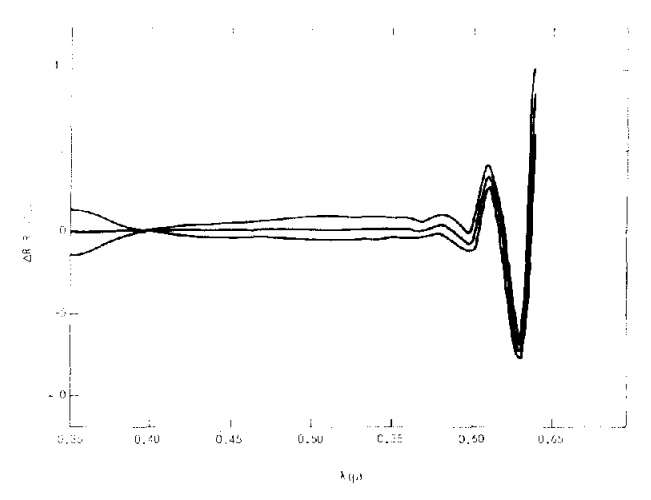


Fig. 3. Error introduced in deriving the reflectivity of a-Si at normal incidence from the normal reflectivity of crystalline silicon and from reflectivity ratios taken at an incidence angle of about 20° for three polarization states: perpendicular, parallel and unpolarized.

Standards at near normal incidence. We plot in Fig. 3 the error between the calculated normal incidence reflectivity of  $\operatorname{a-SiH}_x$  and the normal incidence reflectivity inferred from the ratio of the film signal to that of the standard. As can be seen from Fig. 3, the error is small and insensitive to polarization except where fringes start to appear. The success of this technique depends on the similarity between the refractive indices of crystalline silicon and  $\operatorname{a-SiH}_x$ .

# 3.3. Photoconductivity measurements

A convenient method for obtaining  $\alpha D$  at very low values is photoconductivity. In order to avoid ambiguities due to variable response times we used d.c. measurements. The photocurrent is given by

$$I_{\rm pc} = {\rm constant}(F\alpha D)^{\gamma}$$
 (22)

where F is the incident light flux and  $\gamma$  is a measure of the recombination kinetics [5]. For r.f. anodic films at substrate temperatures of 240 °C (a-SiH<sub>0.16</sub>),  $\gamma$  = 0.7 and is independent of energy in the energy domain 1.3 - 1.7 eV where we utilized the photoconductivity to derive  $\alpha D$ . We reduced fringes by opening up the slit width of the monochromator. In an earlier publication, low energy data were obscured by the incomplete shielding of higher order diffraction from the monochromator [4].

#### 3.4. Low aD transmission measurements

Figure 4 shows the magnitude of  $-\log_{10} T_{\rm M}$  at the position of fringe minima and maxima. The full curve is the arithmetic average of the extrema but includes the wavelength dependence of the baseline as well. Apart from this, the full curve should be given by eqn. (14) and can be solved for

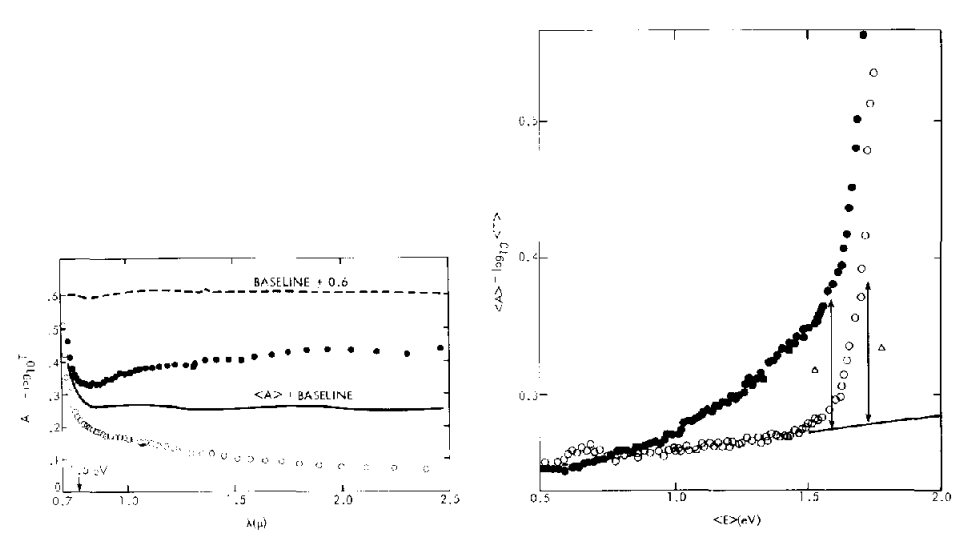


Fig. 4. Extrema of the logarithm of the fringe minima and maxima and their arithmetic average for sample 790402-1 (4.9  $\mu$ m thick): •,  $A_{MIN}$ ;  $^{\circ}$ ,  $A_{MAX}$ .

Fig. 5. Effect of increases in the extinction coefficient  $\alpha$  on the arithmetic average of the logarithm of the transmission minima and maxima (the quantity  $\Delta$  is the difference between eqn. (14a) and eqn. (14b) which is represented as a straight line): •, sample 790330 (4.29  $\mu$ m thick); •, sample 790402-1 (4.90  $\mu$ m thick).

 $\exp(-2\alpha D)$  in the weakly absorbing limit. We chose to subtract eqn. (14) with  $\alpha = 0$ , i.e.

$$T_{\rm F}^{\circ}({\rm I}) = \frac{(1 - R_1)(1 - R_0)}{1 - R_0 R_1} = 1 - R_{\rm F}^{\circ}({\rm I})$$
 (14b)

from  $-\log_{10}\{T_{\rm M}({\rm MAX})T_{\rm M}({\rm MIN})\}^{1/2}$ . This subtraction is shown for two films in Fig. 5. The derived  $\langle \alpha D \rangle/D$  for these films is compared with the photoconductivity data and  $T_{\rm M}$  through eqn. (19) in Figs. 6 and 7. The photoconductivity has been vertically shifted, but we believe that the correspondence in activation energy supports the identification of the photoconductivity with optical absorption. In Fig. 7 we note that the optical data saturate. We associated this with a residual scattering loss.

Although the logarithmic average of adjacent fringes is computationally convenient through eqn. (14), it also eliminates some random error induced by noise in Carey traces. With r.f. glow discharge films prepared on anodic substrates at 240 °C, the data shown in Fig. 6 are the data that are usually observed. Figure 7 is exceptional.

## 4. Optical characterization of a-SiH<sub>x</sub>

4.1. Anodic films prepared by r.f. glow on substrates held at 240  $^{\circ}$ C (a-SiH<sub>0.16</sub>)

In Fig. 8 data on n are presented. The full circles are derived from the analysis described by Fig. 2, and the open circles from iteration of reflectivity

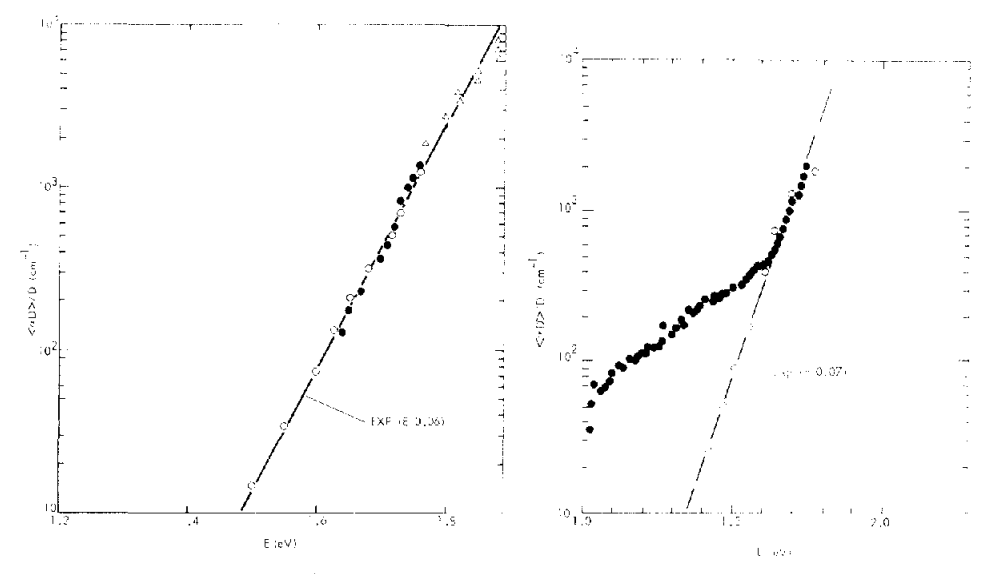


Fig. 6. The derived  $\alpha$  (=  $\langle \alpha D \rangle / D$ ) for sample 790402-1 (4.90  $\mu$ m thick) (one of the films shown in Fig. 5) utilizing eqn. (14a) and eqn. (14b):  $\triangle$ , T;  $\bullet$ ,  $\langle T \rangle$ ;  $\bigcirc$ , photoconductivity.

Fig. 7. The derived  $\alpha$  (=  $\langle \alpha D \rangle / D$ ) for sample 790330 (4.29  $\mu$ m thick) (the other film shown in Fig. 5) utilizing eqn. (14a) and eqn. (14b):  $\bullet$ ,  $\langle T \rangle$ ;  $\circ$ , photoconductivity.

and transmission measurements. Figure 9 shows the absorption constant  $\alpha$  determined by photoconductivity and optical absorption. In Fig. 10 our data are compared with the data of other researchers on films prepared in a similar manner. The a-Si curve is from measurements on an evaporated film by Pierce and Spicer [6]. The pronounced low energy tail presumably corresponds to optically active defects. The tails shown for the measurements of Zanzucchi *et al.* [7] and Tsai and Fritzsche [8] are probably residual scattering losses. The data of Knights [9] cover a smaller energy range than our own but can be associated with a similar exponential absorption.

In Fig. 10 the exponential character of the optical absorption edge on a-SiH $_{0.16}$  is emphasized. There is a remarkable similarity between its optical absorption and that of a variety of amorphous glasses as can be seen from a comparison with amorphous arsenic sulfide (a-As<sub>2</sub>S<sub>3</sub>) [10] in Fig. 10. a-SiH $_x$ , of course, exhibits optimal electronic properties that permit doping and has many of the "classical" semiconducting features that previous amorphous semiconductors lacked.

In Fig. 11 we show composite data derived from all films for the straight-line plot of  $(\alpha E)^{1/2}$  against photon energy. The plot has many features of the more fundamental plot of  $(\epsilon_2 E^2)^{1/2}$  which was first introduced by Tauc et al. [11]. The slope and intercept have a fundamental significance in terms of the optical matrix element and an optical gap  $E_G$ . The curvature at low and high energies establishes a correlation with film thickness. In measuring changes in  $E_G$  with external parameters (preparation or composition variables) it is important to compare films of the same thickness.

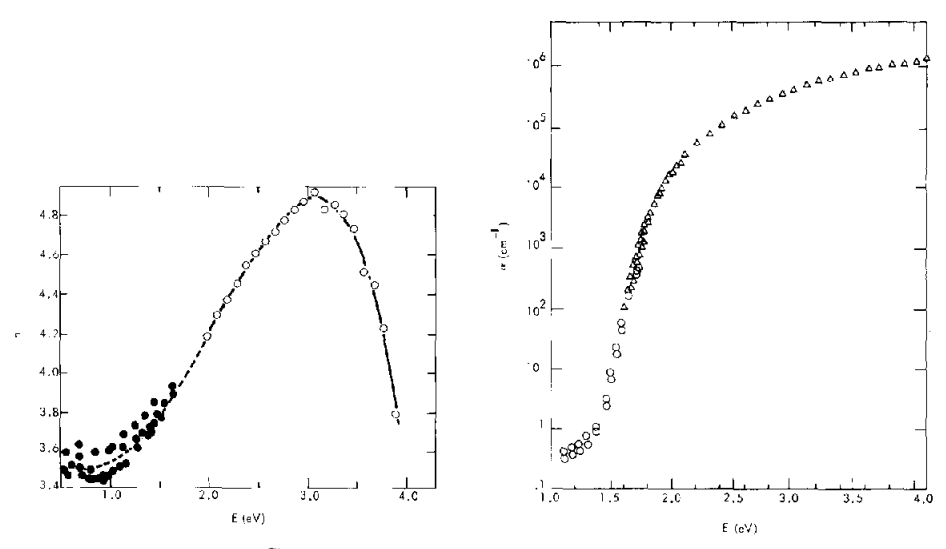


Fig. 8. The real part of  $\tilde{n}$  as a function of photon energy E for a-SiH<sub>0.16</sub>:  $\bullet$ , analysis based on Fig. 2;  $\circ$ , iteration of the reflectivity and transmission (eqns. (19) and (20)).

Fig. 9. Absorption coefficient for a-SiH<sub>0.16</sub> (r.f. glow discharge) derived from optical absorption ( $\triangle$ ) and photoconductivity ( $\bigcirc$ ).

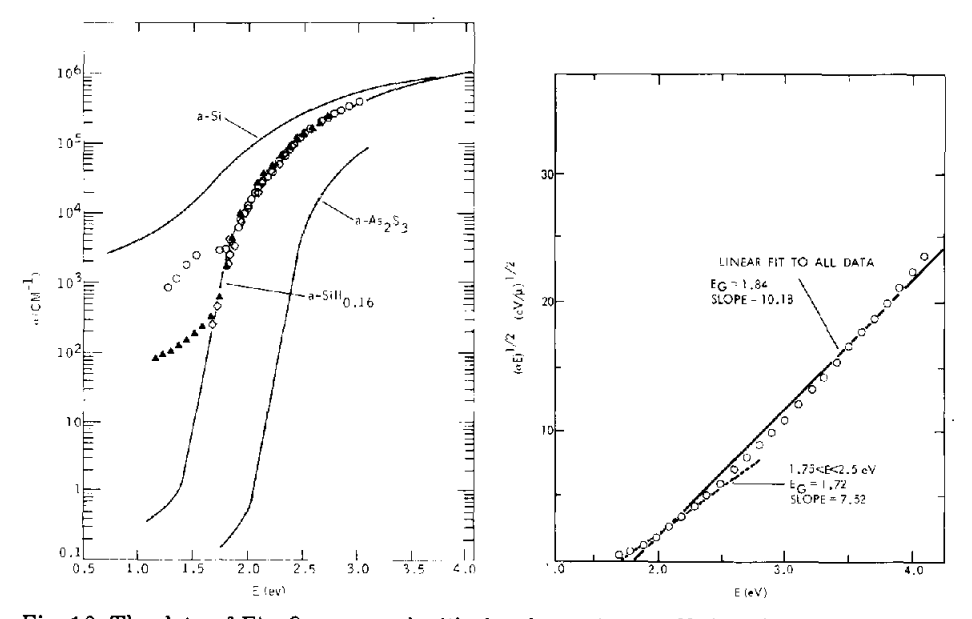


Fig. 10. The data of Fig. 9 compared with the absorption coefficient for evaporated a-Si, as well as r.f. glow discharge films of a-SiH<sub>x</sub> prepared under similar conditions as our own data (the absorption constant for a high quality glass (a-As<sub>2</sub>S<sub>3</sub>) is shown for comparison):  $\Diamond$ , ref. 9;  $\bigcirc$ , ref. 7;  $\blacktriangle$ , ref. 8.

Fig. 11. The data of Fig. 10 plotted in the form suggested by Tauc  $et\ al.$  for optical transitions where momentum is not conserved. This plot is for a variety of films and defines an energy gap  $E_G$  as well as a slope.

# 4.2. The optical gap of a-SiH<sub>x</sub>

Figure 12 shows a typical straight-line plot of  $(\alpha E)^{1/2}$  against energy for a 0.72  $\mu m$  film. These plots are a convenient way of characterizing the material in terms of an optical gap  $E_{\rm G}$  and have a fundamental basis [4]. They are one way of characterizing the material as illustrated in Fig. 13 where  $E_{\rm G}$  is shown as a function of hydrogen concentration for films made in our laboratory (each point represents many films) and similar r.f. films prepared elsewhere [8]. A chemically vapor-deposited film with very small hydrogen content [12] is also shown, as are a variety of reactively sputtered glow discharge films with various hydrogen contents [2]. In all our data the hydrogen content has been measured by the  $^{15}N$  reaction by Lanford [3]. In the other cases, hydrogen evolution has been used.

In Fig. 14 we show the pronounced correlation between the slope of  $(\alpha E)^{1/2}$  with inferred  $E_G$ . Again this correlates with the curvature exhibited in Fig. 11 but can be used advantageously when comparing films of different thicknesses.

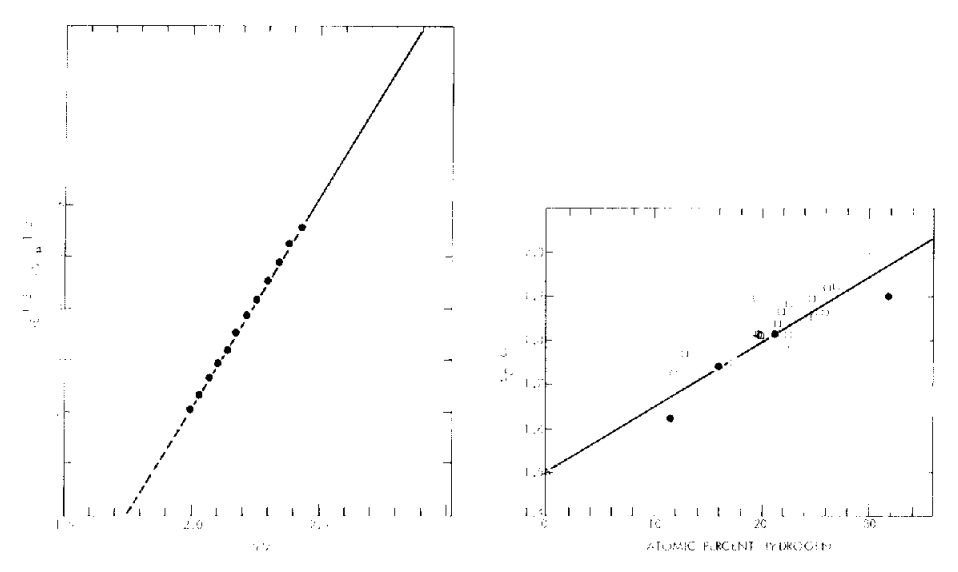


Fig. 12. A similar plot to Fig. 11 but for one particular film (the absence of curvature defines  $E_G$  and slope without ambiguity for films of a comparable thickness): sample 780928-Q;  $D = 0.72 \, \mu \text{m}$ ;  $E_G = 1.74 \, \text{eV}$ ; slope, 8.19.

Fig. 13.  $E_G$  obtained from plots similar to Fig. 12 for r.f. glow discharge samples and reactively sputtered films, in which  $E_G$  increases with the atomic percentage of hydrogen:  $\bullet$ , glow discharge films (Exxon);  $\circ$ , glow discharge films [8];  $\triangle$ , chemically vapor-deposited film with low hydrogen concentration [12].

# 5. Optical characterization of devices

We assume an exponentially falling optical absorption below  $\alpha = 10^3$  cm<sup>-1</sup> for r.f. glow discharge anodic films of a-SiH<sub>0.16</sub> prepared on substrates

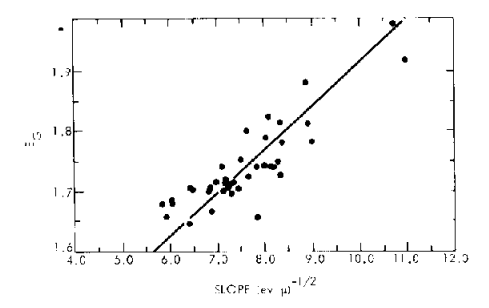


Fig. 14. Measured gap  $E_G$  as a function of slope for a variety of films of different thicknesses. The high gaps correspond to films a few hundred angströms thick and correspond to the high energy data of Fig. 11.

held at 240 °C. An analytic fit to  $\alpha$  is given by (Fig. 11)

$$(\alpha E)^{1/2} = 7.516 (E - 1.716)$$
  $E < 2.178 \text{ eV}$  (23)

$$(\alpha E)^{1/2} = 10.180 (E - 1.837)$$
  $E > 2.178 \text{ eV}$  (24)

We postulate that materials with different hydrogen concentrations have an optical absorption that can be modeled by equations of the form of eqns. (23) and (24) but where we shift the "energy gaps" of eqns. (23) and (24) in a manner appropriate to the data shown in Fig. 13. We thus generate the three curves shown in Fig. 15 which correspond to hypothetical films of a-SiH<sub>0.06</sub> (1.62 eV) and a-SiH<sub>0.22</sub> (1.82 eV) as well as the measured data on a-SiH<sub>0.16</sub> (1.72 eV).

We initially considered an idealized Schottky barrier device consisting of a substrate of either nickel [13] or aluminum [14], a layer of a-SiH<sub>x</sub> of thickness D with arbitrary hydrogen concentration and a metallic contact of 50 Å of palladium. (Our transmission measurements are in good agreement with the palladium data of Johnson and Christy [13].) We calculate at normal incidence the absorption in a distance  $D_{\rm E}$  closest to the palladium. We assume that all the light of a given wavelength that is absorbed in the distance  $D_{\rm E}$  forms electron-hole pairs that can be collected externally with 100% efficiency. We also determine the total reflection coefficient R. For any given ratio of  $D_{\rm E}/D$  we form the ratio A/(1-R) which gives the fraction of the absorbed light at a given wavelength that is collected in the distance  $D_{\rm E}$  for an a-SiH<sub>x</sub> film of thickness D with an absorption coefficient (Fig. 15) appropriate to a given energy gap and hydrogen concentration (Fig. 13).

Figure 16 gives the results for A/(1-R) for a constant  $D_{\rm E}$  and variable D for a-SiH $_{0.16}$  ( $E_{\rm G}$  = 1.72 eV) on a nickel substrate. Figure 17 gives the results for an aluminum substrate where the ratio  $D_{\rm E}/D$  is unity, again for a-SiH $_{0.16}$  ( $E_{\rm G}$  = 1.72 eV). The ripples in the curve arise from interference fringes. In both Figs. 16 and 17 the curves saturate in the blue to 0.87, corresponding to 0.13 absorption in the 50 Å of palladium. We note that, if we compare the two curves for 0.25/0.25, there is an improvement in absorption at long wavelengths produced by the higher reflectivity aluminum substrate.

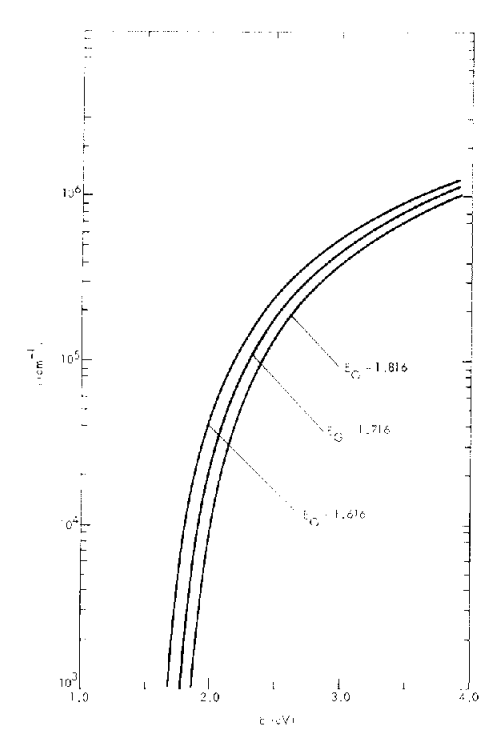


Fig. 15. Idealized absorption curves for a-SiH $_{\rm x}$ . The middle curve corresponds to the two straight-line segments shown in Fig. 11. The other two curves correspond to shifts in the value of  $E_{\rm G}$  without changing the slope.

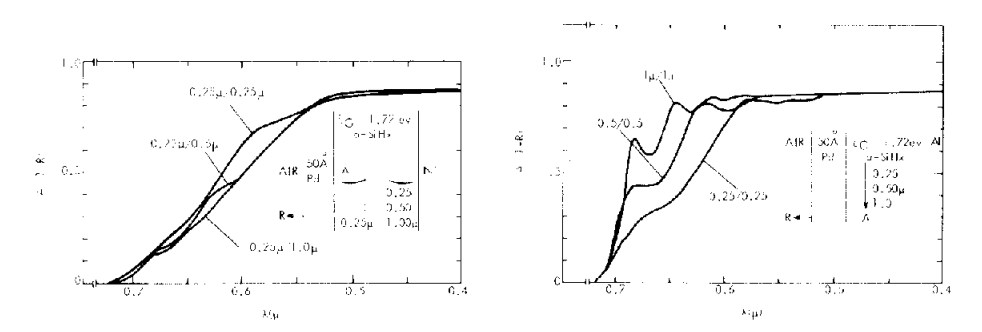


Fig. 16. Calculated fractional absorption in the region closest to the palladium contact for a material with an absorption coefficient corresponding to the middle curve in Fig. 15 and an index corresponding to Fig. 8.

Fig. 17. Calculated fractional absorption in the entire a-SiH $_x$  film as the film thickness is varied on a highly reflecting substrate (aluminum rather than nickel).

If we integrate the curves shown in Figs. 16 and 17 (and also similar curves) with the AM1 spectrum [15], we obtain the data shown in Fig. 18 where the left-hand ordinate is the maximum external current (R=0) that can be obtained for a-SiH<sub>0.16</sub> ( $E_{\rm G}=1.72~{\rm eV}$ ) films of varying ratios of  $D_{\rm E}/D$ 

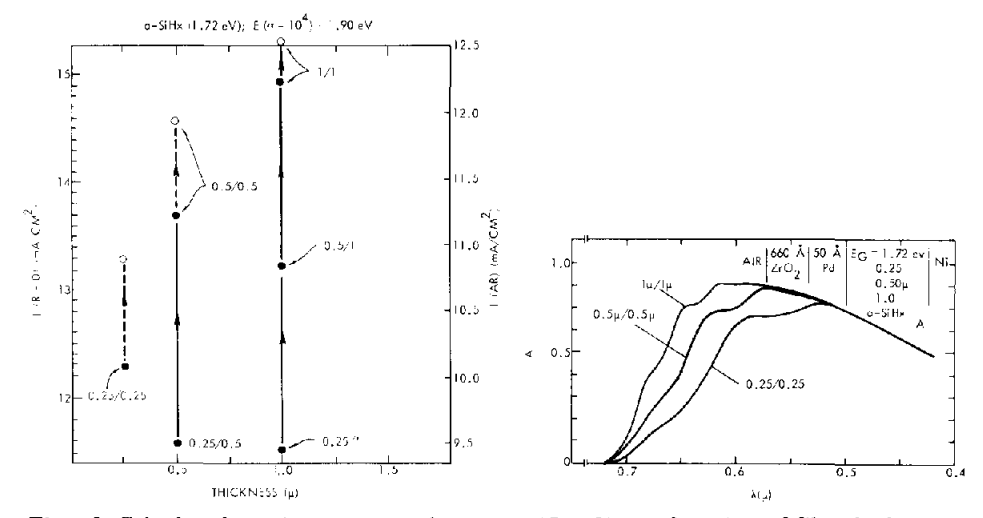


Fig. 18. Calculated maximum external currents (R=0) as a function of film thickness D and collection width  $D_{\rm E}$  expressed as  $D_{\rm E}/D$  for nickel ( $\bullet$ ) (low reflectivity) and aluminum ( $\circ$ ) substrates. The right-hand ordinate reduces this current density by a factor of 0.80 to include losses due to a one-thickness AR coating, as well as 50 Å of palladium.

Fig. 19. Calculated absorption in various thicknesses of a-SiH $_x$  with  $E_{\rm G}$  = 1.72 (Fig. 15) on a nickel substrate.

and different substrates in device configurations that have losses comparable with 50 Å of palladium.

The right-hand ordinate of Fig. 18 represents a scaling of the R=0 data to represent the effect of an antireflection (AR) coating of 660 Å of  $\rm ZrO_2$  [16]. (This thickness is close to but not at the maximum current point.) The scaling is a factor of 0.82 obtained from data similar to those shown in Fig. 19 where A rather than A/(1-R) is plotted as a function of wavelength for the composition shown.

Excellent agreement with Fig. 18 is given by our own measured external short-circuit current of 9.1 mA cm  $^{-2}$  under AM1 for a platinum Schottky barrier device with a 660 Å  $\rm ZrO_2$  AR coating, 50 Å of platinum and a 1.0  $\mu$ m film of a-SiH $_{0.16}$  ( $E_{\rm G}$  = 1.72 eV) [17]. (The calculated transmissions for platinum and palladium are similar.) Electrical evidence suggested a field region of about 3000 Å for this device. It is apparent from Fig. 18 that the assumption of a sharp absorption edge for a-SiH $_x$  severely restricts the short-circuit current for films less than 1  $\mu$ m thick.

In Fig. 20 we show the significant improvements in short-circuit current that may be obtained by reducing the energy gap of a-SiH<sub>x</sub>. Based on Fig. 20, short-circuit currents as high as 16 mA cm<sup>-2</sup> are possible for a-SiH<sub>x</sub> material with  $E_{\rm G}\approx 1.52$  eV ( $H\approx 1\%$ ). If we assume a maximum open-circuit voltage for such material of 1.0 eV and a fill factor of 0.8, the maximum efficiency for a-SiH<sub>x</sub> is 13%. Even allowing for a conservative 10% loss due to shading, the efficiency should be above 10% and certainly competes with the panel efficiencies of present devices. Again it should be emphasized that Figs. 18 and 20 include losses in 50 Å of palladium ( $\approx 20\%$ ).

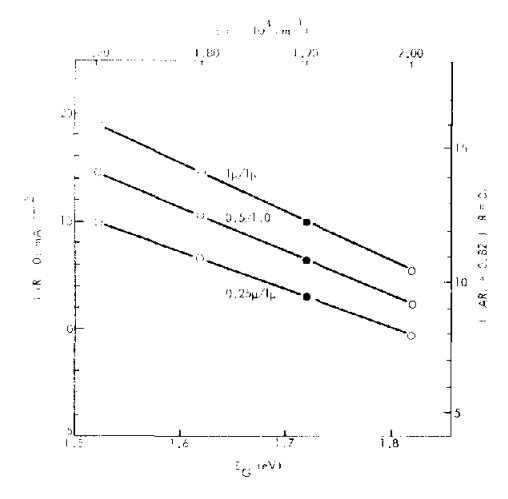


Fig. 20. Calculated maximum (R=0) external short-circuit currents for films 1.0  $\mu$ m thick with the values shown for  $E_G$  and the value of E where  $\alpha = 10^4$  cm<sup>-1</sup>. Again the right-hand ordinate corresponds to a simple AR coating. These data correspond to a nickel substrate. The aluminum substrate improves the currents by about 5%.

## 6. Conclusions

In this paper we focused on the optical properties of a-SiH $_{\rm x}$ . We presented proven techniques for obtaining the fundamental optical constants and showed their value in characterizing the material in terms of an exponential edge and well-defined energy gap  $E_{\rm G}$  which can be related to the hydrogen content of the material. Finally we simulated the optical performance of simple Schottky barrier devices and obtained the optical limitation on device performance. Within the assumptions of this paper the maximum efficiency for the a-Si system is obtained with a hydrogen concentration of a few per cent and should be about 13%. Of course a major challenge is to maintain and improve the electrical properties of the material while improving the optical properties.

# Acknowledgments

We are grateful to J. P. de Neufville, A. Ruppert and T. D. Moustakas for sharing optical data on reactively sputtered films. Most of the films prepared from r.f. glow discharge were made by H. Stasiewski. W. A. Lanford supplied most of the hydrogen analysis.

#### References

- 1 B. Abeles, to be published.
- 2 J. P. de Neufville, T. D. Moustakas, A. F. Ruppert and W. A. Lanford, Proc. 8th Int. Conf. on Amorphous and Liquid Semiconductors, Cambridge, Massachusetts, 1979, in J. Non-Cryst. Solids, 35 - 36 (1980) 481.

- 3 W. A. Lanford, H. P. Trautvetter, J. F. Ziegler and J. P. Keller, Appl. Phys. Lett., 28 (1976) 566.
- 4 G. D. Cody, B. Abeles, C. R. Wronski, B. Brooks and W. A. Lanford, Proc. 8th Int. Conf. on Amorphous and Liquid Semiconductors, Cambridge, Massachusetts, 1979, in J. Non-Cryst. Solids, 35-36 (1980) 463.
- 5 A. Rose, Concepts in Photoconductivity and Allied Problems, Krieger, Huntington, New York, 1978, p. 41.
- 6 D. T. Pierce and W. E. Spicer, Phys. Rev. B, 5 (1972) 3017.
- 7 P. J. Zanzucchi, C. R. Wronski and D. E. Carlson, J. Appl. Phys., 48 (1978) 5227.
- 8 C. C. Tsai and H. Fritzsche, Sol. Energy Mater., 1 (1979) 29.
- 9 J. C. Knights, Proc. Conf. on Structure and Excitations of Amorphous Solids, Williamsburg, Virginia, 1976, in Am. Inst. Phys. Conf. Proc., 31 (1976) 296.
- 10 F. Kosek and J. Tauc, Czech. J. Phys. B, 20 (1970) 96.
- 11 J. Tauc, R. Grigorovici and A. Vancu, Phys. Status Solidi, 15 (1966) 627.
- 12 M. Janai, D. D. Allred, D. C. Booth and B. O. Seraphin, Sol. Energy Mater., 1 (1979) 11.
- 13 P. B. Johnson and R. W. Christy, Phys. Rev. B, 9 (1974) 5056.
- 14 J. R. Beattie, Physica, 23 (1957) 898.
- 15 A. P. Thomas and M. P. Thekaekara, in Sharing the Sun Solar Technology in the Seventies, Winnipeg, Canada, Vol. 1, American Section of the International Solar Energy Society, Florida, 1976, p. 338.
  - P. Ireland, S. Wagner, L. Kazmerski and R. Hulstrom, Science, 204 (1979) 611.
  - C. Backus (ed.), Solar Cells, IEE Press, New York, 1976, pp. 4 5.
- 16 D. Smith and P. Baumeister, Appl. Opt., 18 (1979) 111.
- 17 C. Wronski, B. Abeles and T. Tiedje, to be published.